AGU ADVANCING EARTH AND SPACE SCIENCES

Geophysical Research Letters

RESEARCH LETTER
10.1029/2024GL109785

Spatiotemporal Characteristics and Physical Drivers of Heatwaves in India

Javid Ahmad Dar[1] and **Tushar Apurv**[1]

[1]Department of Civil Engineering, Indian Institute of Technology Kanpur, Kanpur, Uttar Pradesh, India

Key Points:

- Regions of origin and termination of pre-monsoon heatwaves in India are identified using complex networks and event synchronization
- Majority of heatwaves originate from northwest India and propagate in the northeast or southeast direction
- Heatwaves propagating southwards have larger duration and areal extent and are influenced by El Niño Southern Oscillation

Supporting Information:

Supporting Information may be found in the online version of this article.

Correspondence to:

T. Apurv,
tusharap@iitk.ac.in

Citation:

Dar, J. A., & Apurv, T. (2024). Spatiotemporal characteristics and physical drivers of heatwaves in India. *Geophysical Research Letters*, *51*, e2024GL109785. https://doi.org/10.1029/2024GL109785

Received 15 APR 2024
Accepted 31 JUL 2024

Abstract In this study, we analyze the spatiotemporal patterns of propagation of pre-monsoon heatwaves and their drivers in India. Using complex networks, we find that heatwaves originate most frequently in northwest India and propagate in the northeast or southeast direction. Heatwaves propagating in the northeast direction have a higher intensity, lower moving distance, smaller areal coverage, and shorter duration than heatwaves moving in the southeast. We find that the larger area and duration of heatwaves propagating southeast are a result of development of larger and more persistent high-pressure systems extending over entire northern and eastern India, which are influenced by El Niño Southern Oscillation. On the other hand, higher radiative fluxes and larger heat entrainment in the boundary layer in the heatwaves propagating northeast contribute to their higher intensities.

Plain Language Summary We analyze the spatial patterns of where heatwaves originate and how they spread in the pre-monsoon period in India. We find that most heatwaves originate in northwest India. Some of these heatwaves spread to north and central India while some propagate to south India. Heatwaves in northern and central India have higher intensity and last for a shorter period of time as compared to those which spread to south India. The area and duration of heatwaves moving toward south India are influenced by El Nino events. On the other hand, the intensity of heatwaves of central and north India is higher due to greater shortwave radiation and heat entrainment in the boundary layer.

1. Introduction

Heatwaves are periods of extremely high temperatures that have disastrous repercussions on agriculture (Lobell & Field, 2007), human health (McMichael & Lindgren, 2011), and ecosystems (Horton et al., 2016). Between the years 1998 and 2017, heatwaves were found to be the cause of over 166,000 deaths worldwide (Pascaline & Rowena, 2018). During recent decades the intensity, duration, and frequency of heatwaves have increased in many parts of the world (Perkins et al., 2012). Furthermore, the frequency of intense heatwaves is projected to double if the global average temperatures rise by 2°C due to climate change (Dosio et al., 2018).

The high temperatures of most heatwaves can be attributed to anomalies in the states of atmosphere, land surface, or a combination of both (Wehrli et al., 2019). Anomalous anticyclonic circulation in the middle and upper troposphere is a major factor leading to the occurrence of heatwaves (Black et al., 2004; Meehl & Tebaldi, 2004; Perkins, 2015), which can be influenced by large-scale modes of climate variability (Arblaster & Alexander, 2012; Kenyon & Hegerl, 2008). Besides the atmospheric circulation patterns, heat advected from upwind locations can also act as the source of heatwaves (Miralles et al., 2014; Schumacher et al., 2019). The effects of anticyclonic circulation or advected heat can get amplified by the feedback between land and atmospheric processes; dry soils during heatwaves can lead to an increase in sensible heat flux and low evaporative cooling which can result in warming of near-surface temperature (Alexander, 2011; Ghatak et al., 2017; Mueller & Seneviratne, 2012; Perkins, 2015).

India frequently experiences heatwaves in the pre-monsoon period between the months of March–May (Murari et al., 2015). There has been a significant increase in the number of heatwaves in northwest and southeast India (Rohini et al., 2016; Singh et al., 2021), which has been associated with an increase in the number of mortalities (Mazdiyasni et al., 2017; Singh et al., 2021) and is expected to increase further in future due to climate change (Mishra et al., 2017; Murari et al., 2015; Rohini et al., 2019). The occurrence of heatwaves in India are strongly influenced by El Niño Southern Oscillation (ENSO) with higher occurrences of heatwaves during the El Niño years (Murari et al., 2016; Naveena et al., 2021; Pai et al., 2013). Given the increasing risk posed by heatwaves to the human health and environment, there is an urgent need to improve the understanding of their characteristics

and driving mechanisms in India. Many studies have been performed for analyzing the heatwave mechanisms globally (Liu et al., 2020; Röthlisberger & Papritz, 2023; Zschenderlein et al., 2019), and in India (Devi et al., 2023; Ghatak et al., 2017; Panda et al., 2017; Rohini et al., 2016; van Oldenborgh et al., 2018). However, no studies have been performed for characterizing the spatio-temporal evolution of heatwaves in India, which can be critical for forecasts and early warning (Mondal & Mishra, 2021).

The objective of this study is to perform a comprehensive analysis of the spatiotemporal evolution of pre-monsoon (March–May) heatwaves and their drivers in India. We first use a combination of complex network (CN) theory and Event Synchronization framework (Quian Quiroga et al., 2002) to identify spatial patterns in the origin and propagation of heatwaves. We then use the Connected Components on Multilabel 3D images algorithm (CC3D; William Silversmith, 2021) to track the trajectories of all the heatwave events originating from the identified regions of origin and classify them based on distance traveled and the direction of propagation. Finally, we analyze the differences in the physical drivers of the classified heatwaves using reanalysis data sets.

2. Data and Methods

2.1. Study Region and Data

We use the gridded daily maximum temperature data set having a spatial resolution of $1° \times 1°$ provided by the India Meteorological Department (IMD) for the period 1950–2020 to analyze heatwaves occurring during March to May (Srivastava et al., 2009). We use the IMD data set for identifying heatwave events and analyzing the spatiotemporal evolution of their trajectories. We use the reanalysis data from ERA5-Land (European Centre for Medium-Range Weather Forecasts Reanalysis) data set at the daily scale, having a spatial resolution of $0.1° \times 0.1°$, for analyzing the physical drivers of heatwaves. The variables used from the ERA5-Land data set include 2 m air temperature, net surface longwave radiation, downward surface longwave radiation, net surface shortwave radiation, surface latent heat flux, surface sensible heat flux and soil moisture in the top 0–7 cm (Muñoz Sabater, 2019). The geopotential height, zonal and meridional velocity, boundary layer height and total cloud cover are taken from ERA5 data set having a spatial resolution of $0.25° \times 0.25°$ (Hersbach et al., 2023). We also use Niño 3.4 index time-series provided by National Oceanic and Atmospheric Administration (NOAA) for analyzing the influence of ENSO on Indian heatwaves.

2.2. Heatwave Definition and Characteristics

We define heatwave as a period of at least 3 consecutive days when the daily maximum temperature exceeds the 90th percentile threshold. The 90th percentile threshold is calculated based on daily maximum temperature, centered on a 31-day window (Russo et al., 2014). We define heatwave intensity as the average magnitude by which the daily maximum temperature exceeds the 90th percentile threshold while the duration of the heatwave is the length of time for which daily maximum temperature is higher than the above-mentioned threshold.

2.3. Identification of Regions of Origin and Termination of Heatwaves Using Complex Network

We analyze the spatio-temporal evolution of heatwaves using the CN framework, which has been used in several previous studies for the analysis of extreme events (Boers et al., 2013; Konapala & Mishra, 2017; Malik et al., 2012; Mondal & Mishra, 2021). In this framework, different locations are represented as nodes whereas links are used to represent the extent of synchronization of extreme event occurrence between the locations. We use the Event Synchronization framework to quantify the strength of the links between two locations (Quian Quiroga et al., 2002). We briefly explain the methodology in this section; the detailed explanation can be found in the Supporting Information. We first calculate the dynamic delay between events at each pair of two locations i and j (Equations S1 and S2 in Supporting Information S1). A pair of events occurring at the two locations are considered synchronized if the lag time between the two events is less than the dynamic delay (Equation S4 in Supporting Information S1). This pairwise analysis of heatwave events is applied to all possible pairs of locations to compute synchronization Q_{ij} which is the fraction of synchronized events between the two locations regardless of the location in which the event occurred first (Equation S5 in Supporting Information S1); and the delay q_{ij}, which represents the difference between the number of synchronized events occurring first at location i and those occurring first at location j (Equation S6 in Supporting Information S1). The synchronization and delay matrices are then converted into corresponding adjacency matrices (A^Q and A^q respectively), to identify the strongest

connections in the network using a threshold of 95th percentile (Equation S7 and S8 in Supporting Information S1).

The matrices A^Q and A^q are used to calculate two types of network coefficients, namely degree centrality (DC) and network divergence (ND). The DC of a location is defined as the ratio between the number of possible significant connections that it can have with other locations to the total number of connections (Equation S9 in Supporting Information S1). A higher value of DC of a given location indicates that if a heatwave event occurs in that location, it is more likely to be accompanied by heatwave occurrence in other locations within a period of dynamic delay, which is 5 days in the present study. ND is defined as the difference between the number of incoming and outgoing connections in a location (Equation S10 in Supporting Information S1). A negative value of ND signifies a higher number of outgoing connections from a given location in comparison to incoming connections. Conversely, a positive value of ND for a location signifies a greater number of incoming connections as compared to outgoing connections. Therefore, locations exhibiting significant magnitudes of negative and positive values of ND act as regions of origin and termination of heatwaves respectively.

2.4. Identification and Classification of Heatwave Trajectories

We used a 3-D connected component (CC3D) algorithm (William Silversmith, 2021) for tracking heatwaves in space and time. The maximum temperature time-series at all locations are first converted to a binary time-series using the heatwave identification criteria mentioned in Section 2.2; days satisfying heatwave criteria are assigned a value of 1 and 0 otherwise. The CC3D algorithm is applied to the binary time series to identify grid points in the temperature data set, in both space and time, which are a part of the same heatwave event. The algorithm uses a screening window of 3×3 grids which traverses all latitudes and longitudes at each time step. For a given 3×3 window centered at location (i, j), 26 grid points are considered as candidates; 8 surrounding grids on day t and 9 grid points including the point (i, j) and its 8 neighbors on days $t - 1$ and $t + 1$ (Luo, Lau, et al., 2022; Luo, Wang, et al., 2022; Reddy et al., 2022). Any new heatwave-prone grid identified in the screening window is assigned the same label as the existing heatwave-prone grids in the screening window, whereas a new label is assigned to it if there are no heatwave-prone grids in the neighborhood. After this procedure is implemented for all locations at time t, the same procedure is repeated for the next time step. The centroid of heatwave on a given day is calculated as the average of geographical coordinates (i.e., latitude and longitude) identified to be a part of the same event weighted by the intensity of heatwave at each location. The set of locations of heatwave centroids on different days represents the heatwave trajectory.

We first identify the dominant regions of origin of heatwaves in India using the delay matrix (Section 2.3) and cluster the trajectories of heatwaves originating in this region. We consider only the heatwaves whose spatial extent is greater than 8 grids of $1° \times 1°$ resolution (i.e., approx. 96,800 km^2) for clustering analysis in order to avoid heatwave events which do not propagate significantly in space. We classify the heatwave trajectories originating from the dominant regions of origin based on their moving direction and distance (Luo, Wang, et al., 2022) using K-means clustering (Hartigan & Wong, 1979). The optimum number of clusters are determined using silhouette score (Pham et al., 2005). After clustering we also analyze other characteristics of heatwave trajectories such as intensity, total area, lifetime, moving distance and direction (Table S1 in Supporting Information S1).

2.5. Analysis of Energy Fluxes During Heatwaves

In a recent study, Röthlisberger and Papritz (2023) quantified the contributions of diabatic, adiabatic and advective processes to temperature rise during the hottest days of the year globally. They found that diabatic processes are the dominant contributors to temperature rise during heatwaves in India. Therefore, we analyzed the components of the surface energy budget, namely net shortwave radiation, net longwave radiation, sensible heat flux and latent heat flux using the ERA5-Land data set. In this study we consider net shortwave, downward and upward longwave radiation as positive downwards and sensible and latent heat flux as positive upwards.

We use the daily maximum temperature data from IMD to calculate the beginning and ending dates of heatwaves. We then use 2 m-daily maximum temperature data from ERA5-Land data set to identify heatwave locations within ± 1 day of the heatwave dates obtained using the IMD data set. Heatwaves identified from the ERA5-Land are considered only if their spatial extent have an overlap of greater than 80% with the heatwave locations identified using the IMD data set.

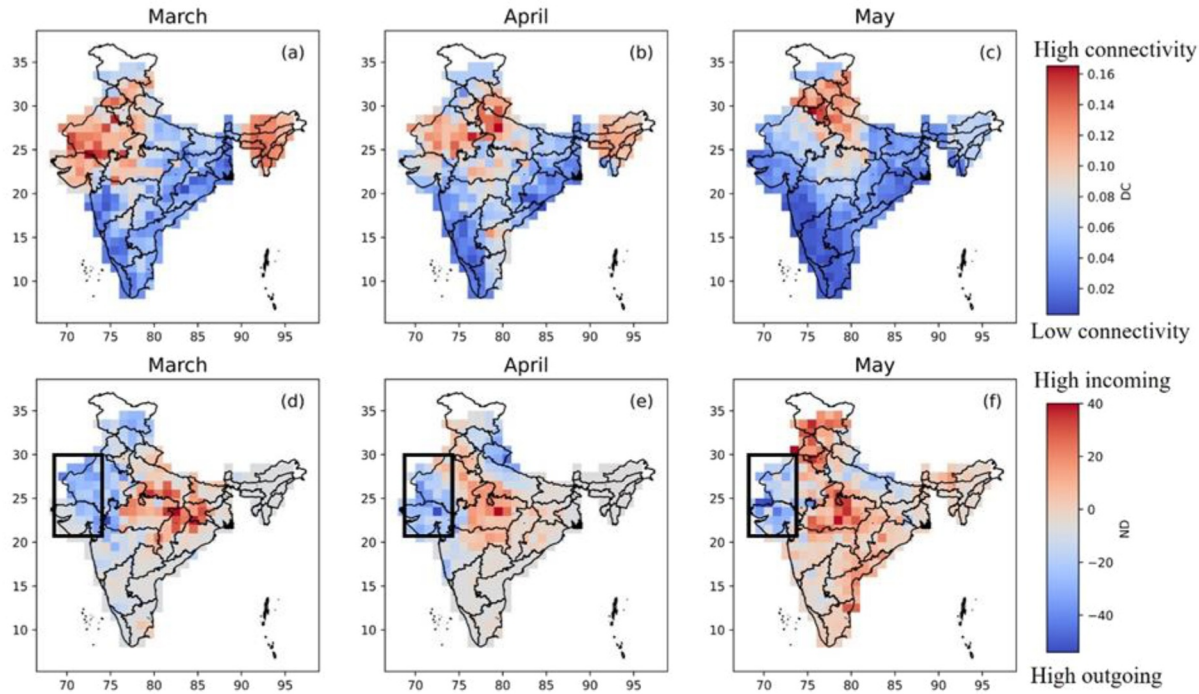

Figure 1. Spatial distribution of degree centrality in panels (a) March, (b) April, and (c) May and network divergence in panels (d) March, (e) April, and (f) May. The rectangular box shows the identified dominant region of origin.

3. Results

3.1. Heatwave Networks

Figures 1a–1c show the values of DC for the months of March to May, with red-colored regions denoting regions with high DC values and hence larger spatial synchronization of heatwaves. As the figure shows, the regions of northwestern and central India have higher values for all months. The values of DC over these regions are greater than 0.1, implying that heatwaves in these regions are synchronized over areas greater than roughly 10% of the area of the country (which is approximately 400,000 km^2). The southern region of India has consistently low values of DC throughout this period, indicating that heatwaves in this region have lower degree of spatial synchronization. The high value of DC in the northwest and central part of India can be attributed to the anticyclonic conditions which develop over this region during pre-monsoon (Ratnam et al., 2016). Similarly, Figures 1d–1f show the ND values for the months of March to May. Negative values of ND can be found in northwest India, suggesting that many heatwaves originate in this region. Conversely, the central and southeastern parts of India show positive ND values, indicating that heatwaves propagate to these regions during the pre-monsoon period. It is interesting to note that the high DC region moves away from the region of origin in northwest India in May due to the larger areal propagation of heatwaves in this month (Figure S2 in Supporting Information S1). Thus, heatwaves originate predominantly in northwest India in all the 3 months and propagate to central India in March and April and southeastern India in May. In the following sections, we analyze the trajectories and drivers of heatwaves emerging from the dominant region of origin identified in northwest India, shown as boxes in Figures 1d–1f.

3.2. Heatwave Trajectories

We identified 80 heatwaves which originated from the dominant region of origin identified in Figure 1, which had a spatial extent larger than 8 grids of $1° \times 1°$ resolution and identified their trajectories using the CC3D algorithm. The trajectories were clustered by k means clustering based on their propagation direction and distance. The optimum number of clusters was found to be 2 based on the Silhouette score (Figure S1 in Supporting Information S1). As shown in Figure 2a, 53 heatwaves are classified as a part of the first cluster which are northeastward propagating (NEP) and 27 heatwaves are classified in the second cluster which are southeastward

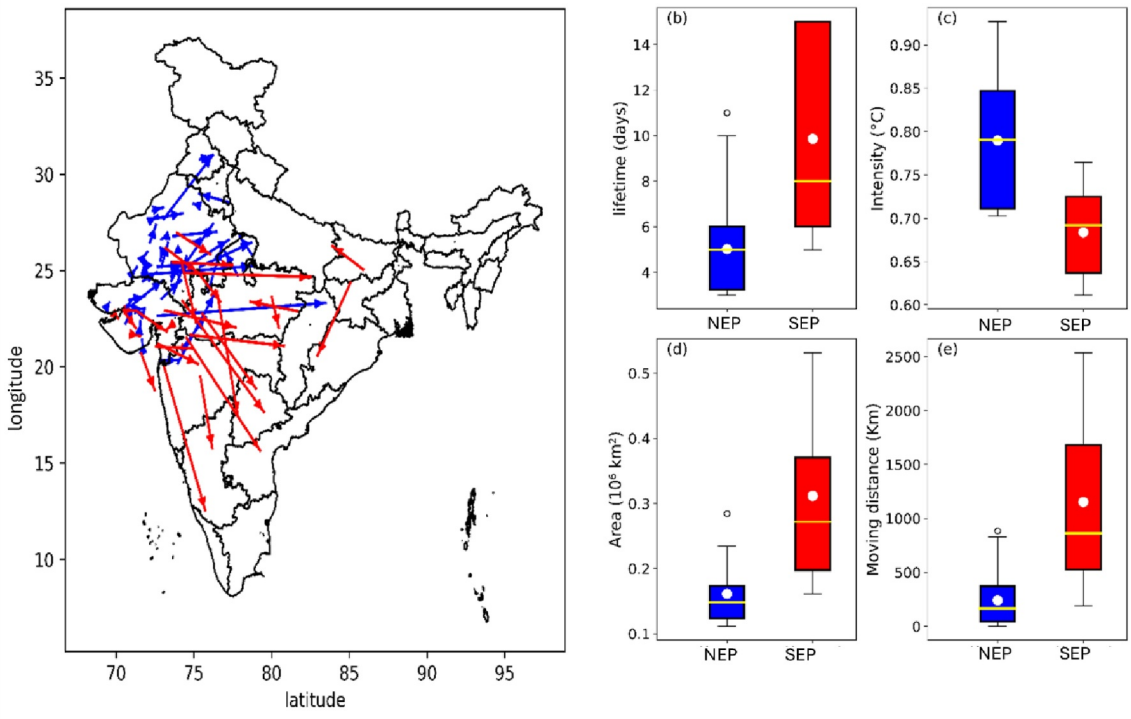

Figure 2. (a) The arrows show the direction of movement of NEP (blue) and SEP (red) heatwaves. The end points of the arrow represent centroid location of the heatwave in the first half and second half of the event with the arrow pointing toward the latter. (b–e) Represents the boxplots of lifetime, intensity, area and moving distance respectively with blue for NEP and red for SEP heatwaves. The white dot is the mean value of each boxplot.

propagating (SEP). The NEP heatwaves are shown in blue and SEP heatwaves are shown in red in Figure 2a. NEP heatwaves exhibit higher intensity, with a mean value of 0.79°C and a median value of 0.78°C, whereas heatwaves that propagate toward the southeast have a comparatively lower intensity with a mean value of 0.68°C and a median value of 0.69°C (Figure 2c). However, SEP heatwaves have longer duration (Figure 2b), larger spatial coverage (Figure 2d), and a larger moving distance as compared to NEP heatwaves (Figure 2e).

3.3. Drivers of Heatwaves

We analyze the relationship of heatwave characteristics in the two clusters with the Niño3.4 index from December to February (DJF) and March to May (MAM) to quantify the influence of El Niño events, following Luo, Wang et al. (2022) and Luo, Lau, et al. (2022). NEP heatwave characteristics did not show any significant correlation with DJF Niño3.4 (Figure S3 in Supporting Information S1). Whereas duration and areal extent of SEP had a significant positive correlation with DJF Niño3.4 with values of 0.40 and 0.58 respectively (Figure S4 in Supporting Information S1). The results for MAM were similar in the case of DJF Niño3.4 (Figures S5 and S6 in Supporting Information S1). These results indicate that ENSO can play a significant role in the longer duration and larger spatial extent of SEP heatwaves.

We further conducted a composite analysis of geopotential height and wind velocity anomalies at 500 hPa for both clusters. Figure 3 shows that both clusters have high positive geopotential height anomalies that develop over northwest India prior to the day of occurrence. We find that the positive geopotential height anomalies for SEP heatwaves have a greater spatial extent, covering almost the entire country to the north of 25°N, and persist for a longer period as compared to NEP heatwaves, which explains the larger spatial extent and duration of SEP heatwaves. Furthermore, SEP heatwaves are accompanied by stronger northerly wind anomalies which results in more southward propagation of the heatwaves.

Out of the 80 heatwave events which emerged from the dominant region of origin identified using the IMD data set (Figure 1), 72 heatwave events were found to coincide with those in ERA5-Land. We compared the intensity of heatwave events calculated from the IMD and ERA5-Land data sets in Figure 4a. We find that there are many

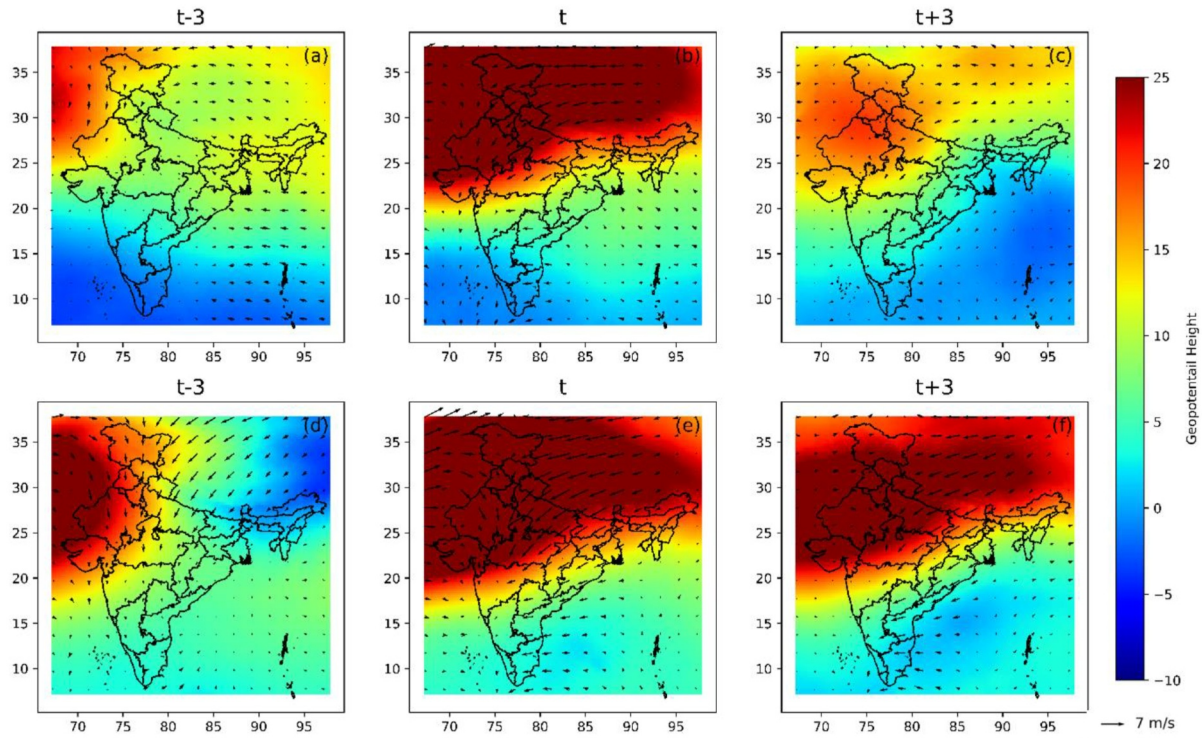

Figure 3. Composite anomalies of geopotential height in meters (shown by colors) and wind velocity meter/sec (shown by arrows) at 500 hPa for NEP (a–c) and SEP (d–f) heatwaves on three days preceding the occurrence ($t-3$), the day of the occurrence (t), and the three days after the occurrence ($t+3$) of heatwaves respectively.

events whose intensities are not well captured in ERA5-Land. Therefore, we analyze the drivers of only those heatwaves for which the error is less than ±0.2°C in the ERA5-Land data set, which results in identification of 54 heatwaves. The threshold error of ±0.2°C was chosen to obtain highest correlation between the intensities from the two data sets while retaining the maximum number of events (Table S2 in Supporting Information S1).

Figure 4 shows the temporal evolution of anomalies of different variables before and after the heatwave onset in blue for NEP heatwaves and red for SEP heatwaves. The box plots show the anomalies across all locations and events in the two clusters. Both clusters of heatwaves show high positive anomalies of net shortwave radiation (Figure 4b) while the anomalies of downward longwave radiation (Figure 4c) are quite small. The net shortwave radiation anomalies are significantly higher for NEP heatwaves, which heats up the land and leads to higher longwave radiation emitted from the surface (more negative anomalies in Figure 4e). As a result, the net radiation anomalies (sum of net shortwave and net longwave radiation) are similar in the two clusters (Figure 4d). The high anomalies of net shortwave radiation in NEP can be attributed to more negative anomalies of cloud cover in NEP as compared to SEP with statistically significant difference on the day of heatwave occurrence (Figure S7a in Supporting Information S1). We further observe that there is a more rapid drying of soil moisture in NEP heatwaves (Figure S7b in Supporting Information S1), which leads to slightly more positive sensible heat flux anomalies (Figure 4f) and more negative latent heat flux anomalies (Figure 4g), although the differences between the two clusters are not statistically significant. We also find that the boundary layer heights in NEP heatwaves are higher than those in SEP heatwaves, and progressively increase up to the heatwave onset, both in terms of absolute height (Figure 4h) and anomaly (Figure S9 in Supporting Information S1), which could be due to the stronger sensible heating in NEP heatwaves. The boundary layer growth can contribute to heat entrainment and accumulation in the boundary layer (Miralles et al., 2014). Thus, the higher intensity of NEP heatwaves could be due to the combined effect of higher upward longwave radiation driven by heating of land surface from shortwave radiation and heat entrainment in the boundary layer.

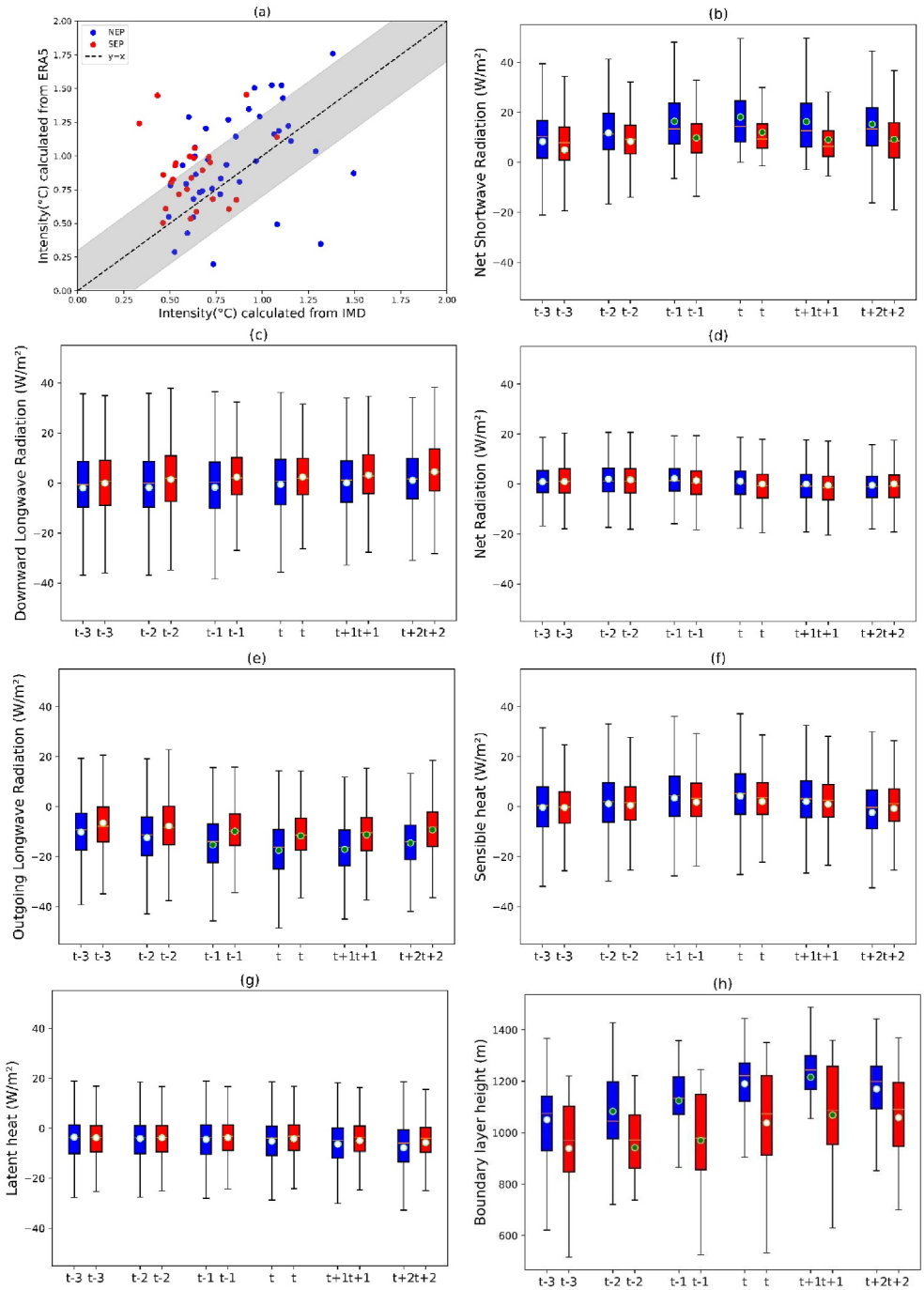

Figure 4. (a) Comparison of heatwave intensities calculated using India Meteorological Department and ERA5-Land data sets with the area shaded in gray representing the events which were considered for analysis. Temporal evolution of anomalies of panel (b) net shortwave radiation (c) downward longwave radiation (d) net radiation (e) outgoing longwave radiation (f) latent heat flux (g) sensible heat flux and (h) actual values of boundary layer height for NEP (blue) and SEP (red) heatwaves. The box plots show anomalies calculated for all heatwave events originating from the dominant regions of origin with "*t*" denoting the day of occurrence of heatwave. The circles represent the mean of each box plot and those filled in green indicate significant difference in anomalies between two clusters at 5% significance using Kruskal-Wallis test.

4. Discussion

We show that India's northwest region serves as the dominant region of origin for heatwaves in India, a significant fraction of which propagate to southern India. The existence of such strong linkages between the two regions identified in our study can be leveraged for issuing early warning for mitigating the impacts of heatwave events in south India based on the heatwave occurrence in the region of origin. Furthermore, we find that the areal extent and duration of the heatwaves which propagate in the southeast direction, are strongly correlated with the Niño 3.4 index in the preceding winter (Figure S3 in Supporting Information S1) and their probability of occurrence is higher during strong El Niño events (Figure S8 in Supporting Information S1), which is consistent with the study by Jaswal et al. (2015). Therefore, there is a significant potential for forecasting heatwaves in south India based on El Niño conditions in the preceding winter (Jaswal et al., 2015).

Previous studies have highlighted the role of enhanced incoming radiation in heatwaves in India (Joshi et al., 2020; Rohini et al., 2016), which agree with our findings. We further show that the shortwave radiation anomalies are higher in north Indian heatwaves, heating the land surface and in turn leading to heating of air through the longwave radiation emitted by the land surface (Figures 4b and 4e). Furthermore, boundary layer growth also contributes to higher temperatures via heat entrainment and accumulation in north Indian heatwaves, which have a smaller propagation distance and are relatively more stationary.

Since we are using reanalysis data set for analysis of physical drivers of heatwaves, we compared the timing, spatial extent and intensities of heatwave events identified using the IMD and ERA5-Land data set and only analyzed those events which are well captured in the ERA5-Land data set. It is interesting to note that while the spatial extent and timing of heatwaves were quite similar in the two data sets for most events (72 out of 80), there were significant discrepancies between the intensities of heatwaves, particularly for the high intensity heatwave events (Figure 4a), for which differences in resolution of the two data sets could also be a contributing factor. These findings highlight the importance of validating reanalysis data sets with available observations for extreme event studies.

5. Conclusion

We find that most of the pre-monsoon heatwaves in India originate from northwest India. Heatwaves originating from this region also have the largest spatial coverage in the country. We identified two dominant trajectories of heatwaves originating from this region: one propagating in the northeast direction and the other in the southeast. Heatwaves propagating in the northeast direction have higher intensity, but lower moving distance and duration as compared to the heatwaves propagating toward south India. The larger area and duration of heatwaves propagating southeast are strongly influenced by El Niño events while larger radiative flux anomalies and heat entrainment in the boundary layer contribute to higher intensities of heatwaves propagating northeast.

Data Availability Statement

The variables used from ERA5-Land are available via Muñoz Sabater, 2019. The data from ERA5 is available via Hersbach et al. (2023). The CC3D library used for tracking heatwaves is available via William Silversmith. (2021). The maximum daily temperature data was taken from the IMD website: https://www.imdpune.gov.in/cmpg/Griddata/Max_1_Bin.html. The Niño 3.4 index used in the study is taken from the National Oceanic and Atmospheric Administration website: https://origin.cpc.ncep.noaa.gov/products/analysis_monitoring/ensostuff/ONI_v5.php.

Acknowledgments
The authors are grateful for the funding provided by Science and Engineering Research Board (SERB), Department of Science and Technology, Government of India (Project number SRG/2021/000452) and the Ministry of Education, India for providing PhD funding through the PMRF program. We thank the two anonymous reviewers for their valuable comments which significantly improved the quality of the paper.

References

Alexander, L. (2011). Extreme heat rooted in dry soils. *Nature Geoscience*, *4*(1), 12–13. https://doi.org/10.1038/ngeo1045

Arblaster, J. M., & Alexander, L. V. (2012). The impact of the El Niño-Southern Oscillation on maximum temperature extremes. *Geophysical Research Letters*, *39*(20). https://doi.org/10.1029/2012GL053409

Black, E., Blackburn, M., Harrison, G., Hoskins, B., & Methven, J. (2004). Factors contributing to the summer 2003 European heatwave. *Weather*, *59*(8), 217–223. https://doi.org/10.1256/wea.74.04

Boers, N., Bookhagen, B., Marwan, N., Kurths, J., & Marengo, J. (2013). Complex networks identify spatial patterns of extreme rainfall events of the South American Monsoon System. *Geophysical Research Letters*, *40*(16), 4386–4392. https://doi.org/10.1002/grl.50681

Devi, R., Gouda, K. C., & Lenka, S. (2023). Analysis of heat wave over different physiographical regions in India. *Theoretical and Applied Climatology*, *154*(3–4), 1343–1356. https://doi.org/10.1007/s00704-023-04639-2

Dosio, A., Mentaschi, L., Fischer, E. M., & Wyser, K. (2018). Extreme heat waves under 1.5°C and 2°C global warming. *Environmental Research Letters*, *13*(5), 054006. https://doi.org/10.1088/1748-9326/aab827

Ghatak, D., Zaitchik, B., Hain, C., & Anderson, M. (2017). The role of local heating in the 2015 Indian Heat Wave. *Scientific Reports*, *7*(1), 7707. https://doi.org/10.1038/s41598-017-07956-5

Hartigan, J. A., & Wong, M. A. (1979). Algorithm AS 136: A K-means clustering algorithm. *Applied Statistics*, *28*(1), 100. https://doi.org/10.2307/2346830

Hersbach, H., Bell, B., Berrisford, P., Biavati, G., Horányi, A., Muñoz Sabater, J., et al. (2023). ERA5 hourly data on pressure levels from 1940 to present [Dataset]. *Copernicus Climate Change Service (C3S) Climate Data Store (CDS)*. https://doi.org/10.24381/cds.bd0915c6

Horton, R. M., Mankin, J. S., Lesk, C., Coffel, E., & Raymond, C. (2016). A review of recent advances in Research on extreme heat events. *Current Climate Change Reports*, *2*(4), 242–259. https://doi.org/10.1007/s40641-016-0042-x

Jaswal, A. K., Rao, P. C. S., & Singh, V. (2015). Climatology and trends of summer high temperature days in India during 1969–2013. *Journal of Earth System Science*, *124*(1), 1–15. https://doi.org/10.1007/s12040-014-0535-8

Joshi, M. K., Rai, A., Kulkarni, A., & Kucharski, F. (2020). Assessing changes in characteristics of hot extremes over India in a warming environment and their driving mechanisms. *Scientific Reports*, *10*(1), 2631. https://doi.org/10.1038/s41598-020-59427-z

Kenyon, J., & Hegerl, G. C. (2008). Influence of modes of climate variability on global temperature extremes. *Journal of Climate*, *21*(15), 3872–3889. https://doi.org/10.1175/2008JCLI2125.1

Konapala, G., & Mishra, A. (2017). Review of complex networks application in hydroclimatic extremes with an implementation to characterize spatio-temporal drought propagation in continental USA. *Journal of Hydrology*, *555*, 600–620. https://doi.org/10.1016/j.jhydrol.2017.10.033

Liu, X., He, B., Guo, L., Huang, L., & Chen, D. (2020). Similarities and differences in the mechanisms causing the European summer heatwaves in 2003, 2010, and 2018. *Earth's Future*, *8*(4), e2019EF001386. https://doi.org/10.1029/2019EF001386

Lobell, D. B., & Field, C. B. (2007). Global scale climate–crop yield relationships and the impacts of recent warming. *Environmental Research Letters*, *2*(1), 014002. https://doi.org/10.1088/1748-9326/2/1/014002

Luo, M., Lau, N., Liu, Z., Wu, S., & Wang, X. (2022). An observational investigation of spatiotemporally contiguous heatwaves in China from a 3D perspective. *Geophysical Research Letters*, *49*(6), e2022GL097714. https://doi.org/10.1029/2022GL097714

Luo, M., Wang, X., Dong, N., Zhang, W., Li, J., Wu, S., et al. (2022). Two different propagation patterns of spatiotemporally contiguous heatwaves in China. *Npj Climate and Atmospheric Science*, *5*(1), 89. https://doi.org/10.1038/s41612-022-00313-y

Malik, N., Bookhagen, B., Marwan, N., & Kurths, J. (2012). Analysis of spatial and temporal extreme monsoonal rainfall over South Asia using complex networks. *Climate Dynamics*, *39*(3–4), 971–987. https://doi.org/10.1007/s00382-011-1156-4

Mazdiyasni, O., AghaKouchak, A., Davis, S. J., Madadgar, S., Mehran, A., Ragno, E., et al. (2017). Increasing probability of mortality during Indian heat waves. *Science Advances*, *3*(6), e1700066. https://doi.org/10.1126/sciadv.1700066

McMichael, A. J., & Lindgren, E. (2011). Climate change: Present and future risks to health, and necessary responses. *Journal of Internal Medicine*, *270*(5), 401–413. https://doi.org/10.1111/j.1365-2796.2011.02415.x

Meehl, G. A., & Tebaldi, C. (2004). More intense, more frequent, and longer lasting heat waves in the 21st century. *Science*, *305*(5686), 994–997. https://doi.org/10.1126/science.1098704

Miralles, D. G., Teuling, A. J., van Heerwaarden, C. C., & Vilà-Guerau de Arellano, J. (2014). Mega-heatwave temperatures due to combined soil desiccation and atmospheric heat accumulation. *Nature Geoscience*, *7*(5), 345–349. https://doi.org/10.1038/ngeo2141

Mishra, V., Mukherjee, S., Kumar, R., & Stone, D. A. (2017). Heat wave exposure in India in current, 1.5°C, and 2.0°C worlds. *Environmental Research Letters*, *12*(12), 124012. https://doi.org/10.1088/1748-9326/aa9388

Mondal, S., & Mishra, A. K. (2021). Complex networks reveal heatwave patterns and propagations over the USA. *Geophysical Research Letters*, *48*(2), e2020GL090411. https://doi.org/10.1029/2020GL090411

Mueller, B., & Seneviratne, S. I. (2012). Hot days induced by precipitation deficits at the global scale. *Proceedings of the National Academy of Sciences*, *109*(31), 12398–12403. https://doi.org/10.1073/pnas.1204330109

Muñoz Sabater, J. (2019). ERA5-Land hourly data from 1950 to present [Dataset]. *Copernicus Climate Change Service (C3S) Climate Data Store (CDS)*. https://doi.org/10.24381/cds.e2161bac

Murari, K. K., Ghosh, S., Patwardhan, A., Daly, E., & Salvi, K. (2015). Intensification of future severe heat waves in India and their effect on heat stress and mortality. *Regional Environmental Change*, *15*(4), 569–579. https://doi.org/10.1007/s10113-014-0660-6

Murari, K. K., Sahana, A. S., Daly, E., & Ghosh, S. (2016). The influence of the El Niño southern oscillation on heat waves in India. *Meteorological Applications*, *23*(4), 705–713. https://doi.org/10.1002/met.1594

Naveena, N., Satyanarayana, G. C., Rao, K. K., Umakanth, N., & Srinivas, D. (2021). Heat wave characteristics over India during ENSO events. *Journal of Earth System Science*, *130*(3), 166. https://doi.org/10.1007/s12040-021-01674-3

Pai, D. S., Nair, S., & Ramanathan, A. N. (2013). Long term climatology and trends of heat waves over India during the recent 50 years (1961-2010). *Mausam*, *64*(4), 585–604. https://doi.org/10.54302/mausam.v64i4.742

Panda, D. K., AghaKouchak, A., & Ambast, S. K. (2017). Increasing heat waves and warm spells in India, observed from a multiaspect framework. *Journal of Geophysical Research: Atmospheres*, *122*(7), 3837–3858. https://doi.org/10.1002/2016JD026292

Pascaline, W., & Rowena, H. (2018). Economic losses, poverty and disaster 1998–2017. In *Report for the united nations office for disaster risk reduction, Geneva, and center for Research on the epidemiology of disasters, brussels* (p. 33). https://doi.org/10.13140/RG.2.2.35610.08643

Perkins, S. E. (2015). A review on the scientific understanding of heatwaves—Their measurement, driving mechanisms, and changes at the global scale. *Atmospheric Research*, *164–165*, 242–267. https://doi.org/10.1016/j.atmosres.2015.05.014

Perkins, S. E., Alexander, L. V., & Nairn, J. R. (2012). Increasing frequency, intensity and duration of observed global heatwaves and warm spells. *Geophysical Research Letters*, *39*(20), L20714. https://doi.org/10.1029/2012GL053361

Pham, D. T., Dimov, S. S., & Nguyen, C. D. (2005). Selection of *K* in *K* -means clustering. *Proceedings of the Institution of Mechanical Engineers - Part C: Journal of Mechanical Engineering Science*, *219*(1), 103–119. https://doi.org/10.1243/095440605X8298

Quian Quiroga, R., Kreuz, T., & Grassberger, P. (2002). Event synchronization: A simple and fast method to measure synchronicity and time delay patterns. *Physical Review E*, *66*(4), 041904. https://doi.org/10.1103/PhysRevE.66.041904

Ratnam, J. V., Behera, S. K., Ratna, S. B., Rajeevan, M., & Yamagata, T. (2016). Anatomy of Indian heatwaves. *Scientific Reports*, *6*(1), 24395. https://doi.org/10.1038/srep24395

Reddy, P. J., Perkins-Kirkpatrick, S. E., & Sharples, J. J. (2022). Interactive influence of ENSO and IOD on contiguous heatwaves in Australia. *Environmental Research Letters*, *17*(1), 014004. https://doi.org/10.1088/1748-9326/ac3e9a

Rohini, P., Rajeevan, M., & Mukhopadhay, P. (2019). Future projections of heat waves over India from CMIP5 models. *Climate Dynamics*, *53*(1–2), 975–988. https://doi.org/10.1007/s00382-019-04700-9

Rohini, P., Rajeevan, M., & Srivastava, A. K. (2016). On the variability and increasing trends of heat waves over India. *Scientific Reports*, *6*(1), 26153. https://doi.org/10.1038/srep26153

Röthlisberger, M., & Papritz, L. (2023). Quantifying the physical processes leading to atmospheric hot extremes at a global scale. *Nature Geoscience*, *16*(3), 210–216. https://doi.org/10.1038/s41561-023-01126-1

Russo, S., Dosio, A., Graversen, R. G., Sillmann, J., Carrao, H., Dunbar, M. B., et al. (2014). Magnitude of extreme heat waves in present climate and their projection in a warming world. *Journal of Geophysical Research: Atmospheres*, *119*(22), 12500–12512. https://doi.org/10.1002/2014JD022098

Schumacher, D. L., Keune, J., van Heerwaarden, C. C., Vilà-Guerau de Arellano, J., Teuling, A. J., & Miralles, D. G. (2019). Amplification of mega-heatwaves through heat torrents fuelled by upwind drought. *Nature Geoscience*, *12*(9), 712–717. https://doi.org/10.1038/s41561-019-0431-6

Singh, S., Mall, R. K., & Singh, N. (2021). Changing spatio-temporal trends of heat wave and severe heat wave events over India: An emerging health hazard. *International Journal of Climatology*, *41*(S1), E1831–E1845. https://doi.org/10.1002/joc.6814

Srivastava, A. K., Rajeevan, M., & Kshirsagar, S. R. (2009). Development of a high resolution daily gridded temperature data set (1969-2005) for the Indian region. *Atmospheric Science Letters*, *10*(4), 249–254. https://doi.org/10.1002/asl.232

van Oldenborgh, G. J., Philip, S., Kew, S., van Weele, M., Uhe, P., Otto, F., et al. (2018). Extreme heat in India and anthropogenic climate change. *Natural Hazards and Earth System Sciences*, *18*(1), 365–381. https://doi.org/10.5194/nhess-18-365-2018

Wehrli, K., Guillod, B. P., Hauser, M., Leclair, M., & Seneviratne, S. I. (2019). Identifying key driving processes of major recent heat waves. *Journal of Geophysical Research: Atmospheres*, *124*(22), 11746–11765. https://doi.org/10.1029/2019JD030635

William, S. (2021). cc3d: Connected components on Multilabel 3D images. [Software]. https://pypi.org/project/connected-components-3d/

Zschenderlein, P., Fink, A. H., Pfahl, S., & Wernli, H. (2019). Processes determining heat waves across different European climates. *Quarterly Journal of the Royal Meteorological Society*, *145*(724), 2973–2989. https://doi.org/10.1002/qj.3599